Published in final edited form as:
Ophthalmic Surg Lasers Imaging. 2008 ; 39(4 Suppl): S126–S131.

Ultrahigh-resolution Spectral Domain Optical Coherence Tomography Imaging of the Lamina Cribrosa

Larry Kagemann, MS, **Hiroshi Ishikawa, MD**, **Gadi Wollstein, MD**, **Peter M. Brennen, MD**, **Kelly A. Townsend, BS**, **Michelle L. Gabriele, BS**, and **Joel S. Schuman, MD**
From UPMC Eye Center, Eye and Ear Institute, Ophthalmology and Visual Science Research Center, University of Pittsburgh (LK, HI, GW, PMB, KAT, MLG, JSS); the Department of Bioengineering, Swanson School of Engineering, University of Pittsburgh (LK, HI, MLG); and the Center for the Neural Basis of Cognition, Carnegie Mellon University and University of Pittsburgh, Pittsburgh, Pennsylvania (JSS).

Abstract

Study of the structure of the lamina cribrosa is critical in glaucoma research. The purpose of this study is to determine the optimal spectral domain optical coherence tomography imaging protocol for the digital isolation and display of the lamina cribrosa. Three-dimensional datasets centered on the lamina cribrosa were obtained with 200 × 200 to 512 × 512 A-scan densities. The effect of scan density and c-mode slab thickness was subjectively compared. Increasing slab thickness reduced the sharpness of visible prelamina and lamina cribrosa structures. In retrolamina structures, thin slabs provided good visualization, but increased slab size increased the visibility of deeper structures. Scan times as short as 2.3 seconds (256 × 256 A-scans) degraded visualization of the shape of the optic nerve head. The optical scan protocol for lamina cribrosa imaging appears to be a 3 × 3 mm 200 × 200 A-scan volume with the lamina cribrosa positioned near direct current.

INTRODUCTION

The structure of the optic nerve head, and specifically the lamina cribrosa, has been an area of interest in glaucoma research for many years.[1–3] Alterations in its mechanical properties may lead to backward bowing and cupping of the optic disc, potentially blocking retrograde transport of neurotropic factors and ultimately leading to retinal ganglion cell apoptosis.[4–7] Recent application of computer modeling and finite element analysis has increased our understanding of the response of the various tissues within the optic nerve head to elevated intraocular pressure.[8–12] These studies are limited because they were conducted ex vivo in an animal model. To date, it has been impossible to non-invasively image the lamina cribrosa in humans.

Optical coherence tomography (OCT) is a non-invasive imaging technique that has been applied to biological systems.13 The current commercial generation of time domain OCT (TD-OCT) acquires 400 axial scans (A-scans) per second, limiting its use in biological systems to two-dimensional (2D) slices. The advent of spectral domain OCT (SD-OCT) has increased the A-scan acquisition rate to 50,000 A-scans per second.14–17 The high speed of SD-OCT allows the acquisition of reflectance measurements in three-dimensional (3D)

Address correspondence to Joel S. Schuman, MD, UPMC Eye Center, Department of Ophthalmology, University of Pittsburgh School of Medicine, 203 Lothrop Street, Eye and Ear Institute, Suite 816, Pittsburgh, PA 15213.
Dr. Schuman did not participate in the editorial review of this manuscript.

volumes of living tissue with an acceptable amount of movement artifact. Once acquired, it is possible to sample various planes and slabs within the 3D volume for the visualization of embedded structures. The purpose of this study is to determine the optimal SD-OCT imaging protocol for the digital isolation and display of the lamina cribrosa within a 3D SD-OCT dataset centered on the optic nerve head.

TECHNIQUE

All procedures were approved by the institutional review board at the University of Pittsburgh, and informed consent was provided by the subjects before participation in the study. The study was performed in compliance with the tenets of the Declaration of Helsinki and the Health Insurance Portability and Accountability Act.

Imaging Protocol

Three-dimensional spectral imaging reflectance images were obtained from a 3 × 3 × 2-mm volume of tissue centered on the surface of the optic nerve head. The surface of the retinal nerve fiber layer was allowed to “flip” at the top of the frame to position the lamina cribrosa in the area of best image quality (Fig. 1). Each dataset had 1,024 sampling points along each A-scan line covering the 2-mm tissue volume thickness. The 3 × 3-mm lateral area of the tissue volume was imaged at 200 × 200, 256 × 256, 300 × 300, 400 × 400, and 512 × 512 A-scan densities. The effect of scan duration, which increases with A-scan density, was subjectively examined. The duration of slice and volume scans is presented in the Table.

Imaging System

Imaging was performed using a customized SD-OCT. A patient scanner and an optics engine (Bioptigen Inc., Research Triangle Park, North Carolina) were coupled with a quad-diode 200-nm bandwidth broad-lighter centered at 840 nm (Superlum, Carrigtwohill, County Cork, Ireland). With a theoretical axial resolution of 1.6 μm, limitations in the spectrometer yield an actual axial resolution of approximately 2 μm. Raw spectral samples were converted to reflectance data with Bioptigen’s software, which compensates for dispersion in software. The 3D reflectance data were processed for display using customized software of our own design (HI).

Image Processing

Reflectance from three depths within each 3D dataset was isolated for display: superficial/prelamina optic nerve head, lamina cribrosa, and retrolaminar optic nerve head. Tissue planes were marked manually in the horizontal and vertical directions. Tissues continuous with the termination of the retinal pigment epithelium (RPE) were assumed to include the lamina cribrosa (Fig. 2). Prelamina and superficial tissues were considered to be those immediately anterior to the lamina cribrosa and retrolamina tissue immediately posterior to the lamina cribrosa. Images were produced as 2D en face images of the reflectance sample within the above-described slabs with various thicknesses (50–300 μm).

RESULTS

The optic nerve heads of two healthy subjects were imaged: the left eye of a 30-year-old African American woman and the right eye of a 45-year-old white man. Figure 3, A and B, displays the lamina cribrosa level of the optic nerve head using 250- and 70-μm slab thicknesses, respectively.

The effects of increasing the slab size on image quality and content are displayed in Figure 4. Increasing slab thickness reduced the sharpness of visible prelamina and lamina cribrosa

structures. In retrolamina structures, thin slabs provided good visualization, but increased slab size increased the visibility of deeper structures at the cost of sharpness (Fig. 4).

The effect of varying A-scan density is displayed in Figure 5. Scan times increase with A-scan density. Eye motion in scans with a duration of as little as 2.3 seconds (256 × 256 A-scans) degrades visualization of the shape of the optic nerve head, as well as that of the structures within (Fig. 5). Conversely, increasing scan density progressively improves the quality of the cross-sectional frames (Fig. 5, right panel).

DISCUSSION

In this study, we were able to acquire in vivo lamina cribrosa scans with SD-OCT. Images could be obtained across a wide range of A-scan densities, but a 200 × 200 A-scan was sufficiently rapid to minimize eye movements while the scan was being acquired. Regarding analysis of the 3D datasets, thin slabs aligned to the contour of the lamina cribrosa yielded sharp visualization of optic nerve head structures.

Future SD-OCT systems will use complex conjugate resolution technologies to improve SD-OCT imaging. [18,19] Specifically, the length of the axial scan will double from 2 to 4 mm and the location of highest signal strength and resolution will move from one edge of the image frame to the center of the image frame.[18,19] A 4-mm window will allow imaging of the lamina cribrosa without the need to flip surface tissues (Fig. 1). This will allow imaging of specific optic nerve head layers without the appearance of ghost contributions of the surface layers as seen in Figure 4 in the lamina cribrosa images between 10:00 and 12:00, especially with the thinner slabs. These surfaces are clearly visible because, after folding, their reflections appear directly on top of the RPE, which was used as the lamina cribrosa landmark and which is located in the center of the slab (Fig. 4, lamina cribrosa row, slab frame).

There was an obvious trade-off between A-scan density and eye movement. The slower high-density scans contained more eye movements than did faster low-density scans (Fig. 5). Surprisingly, despite the grainy appearance of the slices, 200 × 200 A-scan c-mode images provided satisfactory visualization of optic nerve head structures. Higher-density scans may improve visualization of these structures, but this will require the compensation of eye movements. Without an extraordinarily stable eye, slice alignment routines will be required to minimize the distorting effects of eye movements on 2D lamina cribrosa images in scans longer than 2 seconds. However, even with A-scan densities as high as 1,024 × 1,024, the time to scan any single frame is much less than 1 second (Table).

A majority of frames obtained at high scan densities with the current system appear to have negligible eye motion artifact. Image noise due to eye movements becomes apparent when generating 2D lamina cribrosa images. Individual frames only require a stationary eye throughout the duration of the frame scan (Table), whereas 2D lamina cribrosa images require a stationary eye throughout the duration of the entire 3D volume scan.

Improvements in laser technology may hold the key to future generations of OCT technology capable of imaging the retina with high A-scan densities without noise from eye motion. Huber et al. reported the use of a Fourier domain mode locked light source that enabled A-scan acquisition at a rate of 236,000 scans per second, which is approximately 8.5 times faster than the Bioptigen system. [20] Such a system would allow the acquisition of 512 × 512 A-scan data volumes at a rate of one 3D *volume* per 1.1 seconds, introducing the possibility of 4D imaging, referring to the rapid acquisition of multiple sequential volumes. Minimizing eye movements through speed will result in systems that rapidly produce a large amount of scan data. The effect of scan density on file size is presented in the Table.

Structures of the anterior optic nerve were visualized by sampling 3D reflectance volumes along tissue layer contours. Fast scans (less than 2 seconds) provided 3D datasets relatively free of eye movements. As scan time increased, so did the number of eye movements. Eye movements did not appear to distort individual slices but caused an increasing degree of distortion on 2D lamina cribrosa images. Using the current technology, the optical scan protocol for lamina cribrosa imaging appears to be a 3 × 3 mm 200 × 200 A-scan volume with the lamina cribrosa positioned near direct current (top of the frame) for highest possible signal and resolution.

Acknowledgments

Supported by National Institutes of Health grants R01-EY13178-08, R01-EY11289-22, and P30-EY008098; The Eye and Ear Foundation, Pittsburgh, Pennsylvania; and unrestricted grants from Research to Prevent Blindness, Inc., New York, New York.

Dr. Schuman receives royalties from intellectual property licensed by M.I.T. to Carl Zeiss Meditec, Inc. Dr. Wollstein receives grant support from Carl Zeiss Meditec, Inc., and Optovue.

REFERENCES

1. Lasco F, Nicolesco M. Syndrome of excavation of the lamina cribrosa sclerae: pseudoglaucoma [article in French]. Ophthalmologica 1958;136:90–98. [PubMed: 13578338]
2. Weisse U. Histologic examination of the cribriform plate in glaucoma [article in German]. Ophthalmologica 1964;148:431–441. [PubMed: 14265349]
3. Emery JM, Landis D, Paton D, Boniuk M, Craig JM. The lamina cribrosa in normal and glaucomatous human eyes. Trans Am Acad Ophthalmol Otolaryngol 1974;78:OP290–OP297. [PubMed: 4825057]
4. Quigley HA. The pathogenesis of reversible cupping in congenital glaucoma. Am J Ophthalmol 1977;84:358–370. [PubMed: 900230]
5. Gaasterland D, Tanishima T, Kuwabara T. Axoplasmic flow during chronic experimental glaucoma. 1. Light and electron microscopic studies of the monkey optic nervehead during development of glaucomatous cupping. Invest Ophthalmol Vis Sci 1978;17:838–846. [PubMed: 81192]
6. Quigley HA, Addicks EM. Chronic experimental glaucoma in primates. II. Effect of extended intraocular pressure elevation on optic nerve head and axonal transport. Invest Ophthalmol Vis Sci 1980;19:137–152. [PubMed: 6153173]
7. Quigley HA, Addicks EM. Regional differences in the structure of the lamina cribrosa and their relation to glaucomatous optic nerve damage. Arch Ophthalmol 1981;99:137–143. [PubMed: 7458737]
8. Downs JC, Yang H, Girkin C, et al. Three-dimensional histomorphometry of the normal and early glaucomatous monkey optic nerve head: neural canal and subarachnoid space architecture. Invest Ophthalmol Vis Sci 2007;48:3195–3208. [PubMed: 17591889]
9. Yang H, Downs JC, Bellezza A, Thompson H, Burgoyne CF. 3-D histomorphometry of the normal and early glaucomatous monkey optic nerve head: prelaminar neural tissues and cupping. Invest Ophthalmol Vis Sci 2007;48:5068–5084. [PubMed: 17962459]
10. Burgoyne CF, Downs JC, Bellezza AJ, Suh JK, Hart RT. The optic nerve head as a biomechanical structure: a new paradigm for understanding the role of IOP-related stress and strain in the pathophysiology of glaucomatous optic nerve head damage. Prog Retin Eye Res 2005;24:39–73. [PubMed: 15555526]
11. Burgoyne CF, Downs JC, Bellezza AJ, Hart RT. Three-dimensional reconstruction of normal and early glaucoma monkey optic nerve head connective tissues. Invest Ophthalmol Vis Sci 2004;45:4388–4399. [PubMed: 15557447]
12. Burgoyne CF. Image analysis of optic nerve disease. Eye 2004;18:1207–1213. [PubMed: 15534606]
13. Huang D, Swanson EA, Lin CP, et al. Optical coherence tomography. Science 1991;254:1178–1181. [PubMed: 1957169]

14. Morgner U, Drexler W, Kartner FX, et al. Spectroscopic optical coherence tomography. Opt Lett 2000;25:111–113. [PubMed: 18059799]
15. Wojtkowski M, Kowalczyk A, Leitgeb R, Fercher AF. Full range complex spectral optical coherence tomography technique in eye imaging. Opt Lett 2002;27:1415–1417. [PubMed: 18026464]
16. Yasuno Y, Makita S, Sutoh Y, Itoh M, Yatagai T. Birefringence imaging of human skin by polarization-sensitive spectral interferometric optical coherence tomography. Opt Lett 2002;27:1803–1805. [PubMed: 18033369]
17. de Boer JF, Cense B, Park BH, Pierce MC, Tearney GJ, Bouma BE. Improved signal-to-noise ratio in spectral-domain compared with time-domain optical coherence tomography. Opt Lett 2003;28:2067–2069. [PubMed: 14587817]
18. Tao YK, Zhao M, Izatt JA. High-speed complex conjugate resolved retinal spectral domain optical coherence tomography using sinusoidal phase modulation. Opt Lett 2007;32:2918–2920. [PubMed: 17938652]
19. Sarunic MV, Applegate BE, Izatt JA. Real-time quadrature projection complex conjugate resolved Fourier domain optical coherence tomography. Opt Lett 2006;31:2426–2428. [PubMed: 16880844]
20. Huber R, Adler DC, Srinivasan VJ, Fujimoto JG. Fourier domain mode locking at 1050 nm for ultra-high-speed optical coherence tomography of the human retina at 236,000 axial scans per second. Opt Lett 2007;32:2049–2051. [PubMed: 17632639]

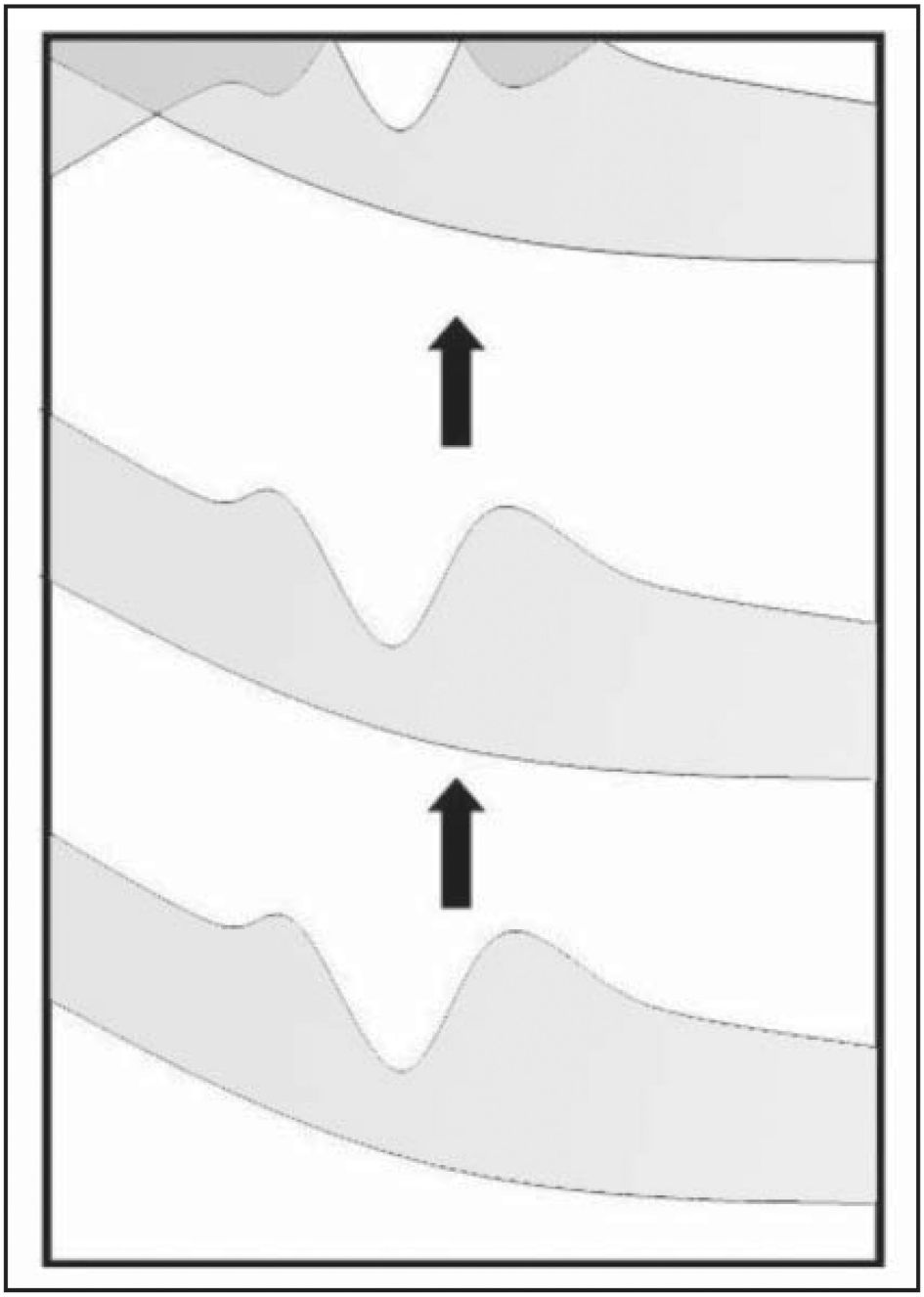

Figure 1.
During alignment, the lamina cribrosa was moved to the area of highest signal strength, even if this resulted in the flipping of the superficial retinal layers, as shown in the upper part of the figure.

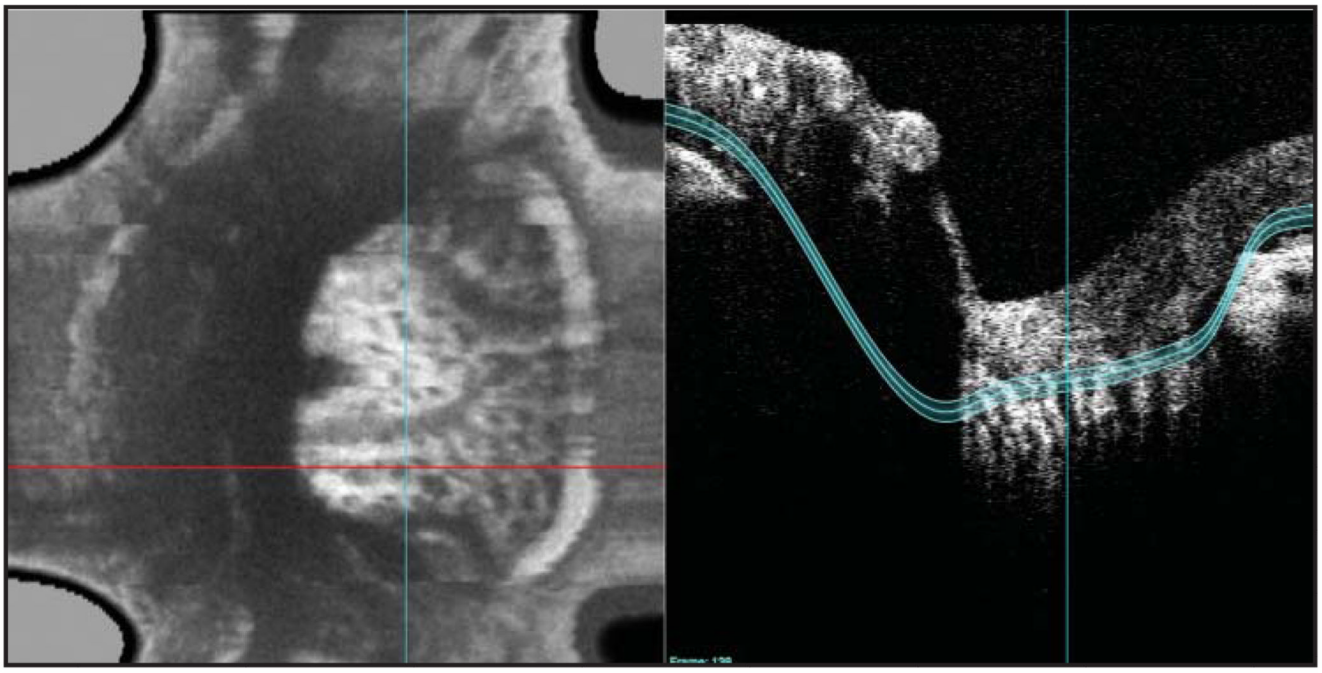

Figure 2.
Contour lines were identified and entered manually based on the observed tissue structures within a slice.

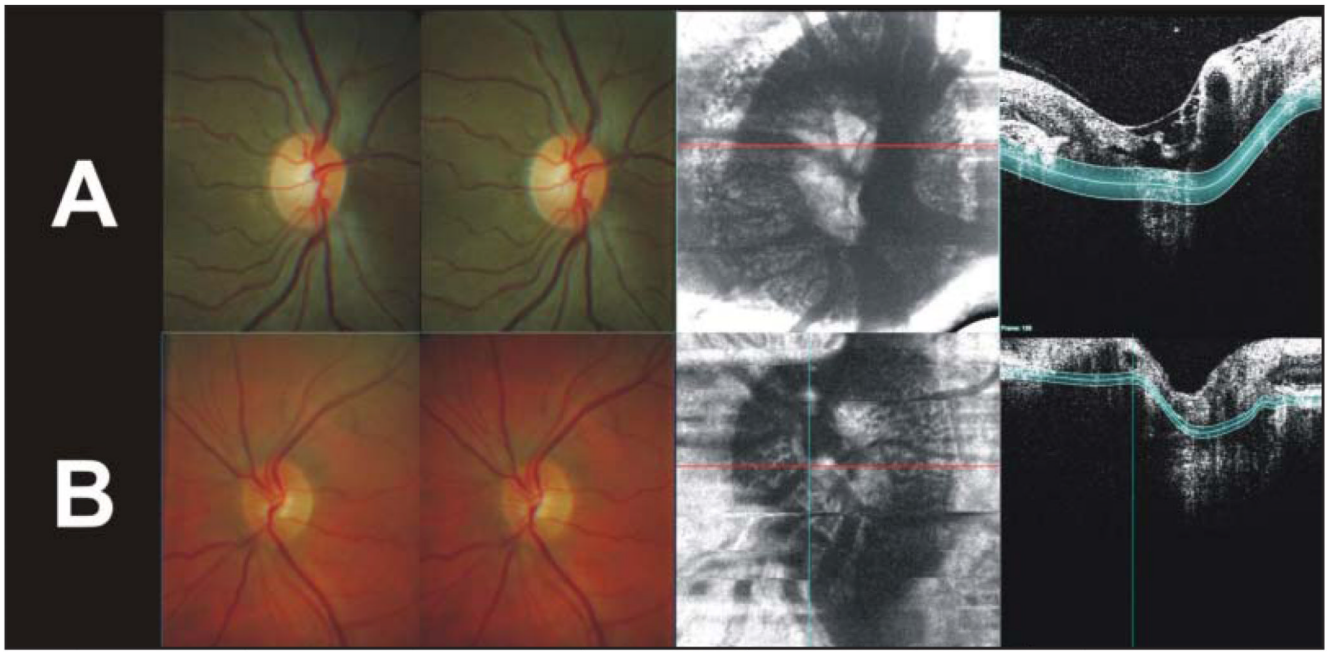

Figure 3.
Crossed stereo optic nerve head images and lamina cribrosa images from the two subjects imaged. A, The left eye of a 30-year-old African American woman using a 250-μm slab thickness. B, The right eye of a 45-year-old white man using a 70-μm slab thickness.

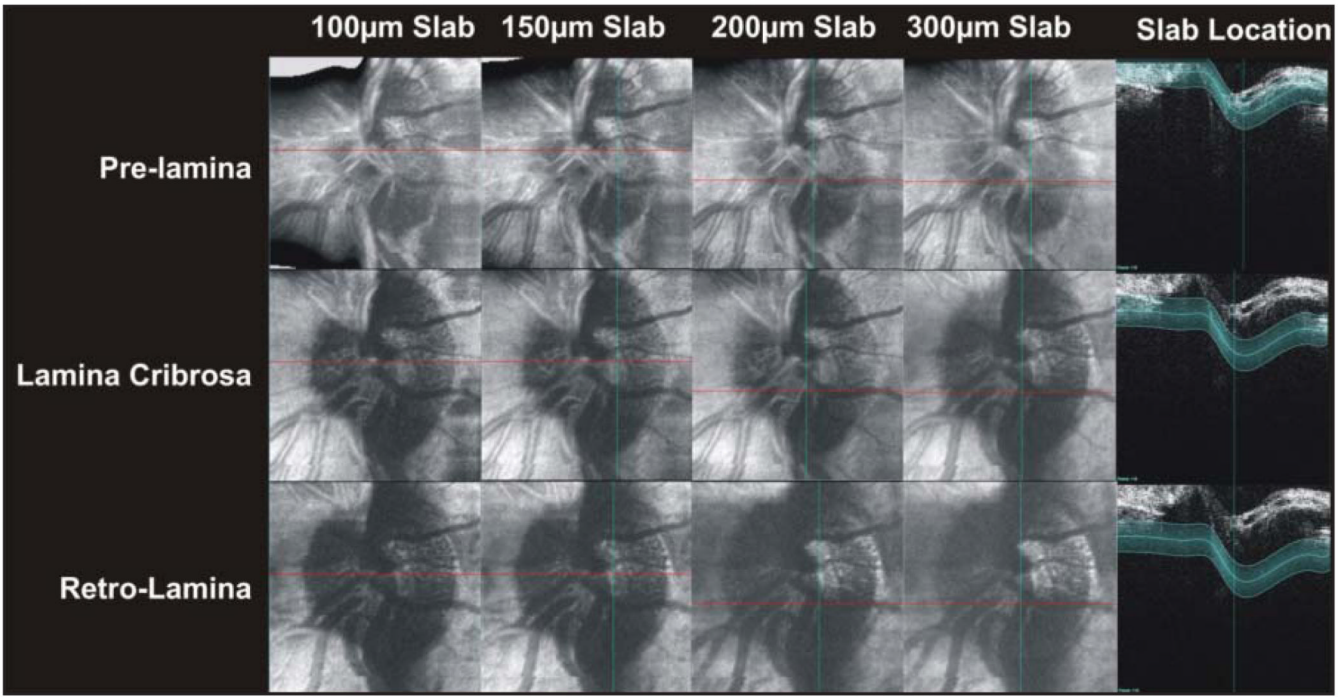

Figure 4.
Side-by-side comparisons of c-mode images resulting from various slab thicknesses at three different levels of the optic nerve head.

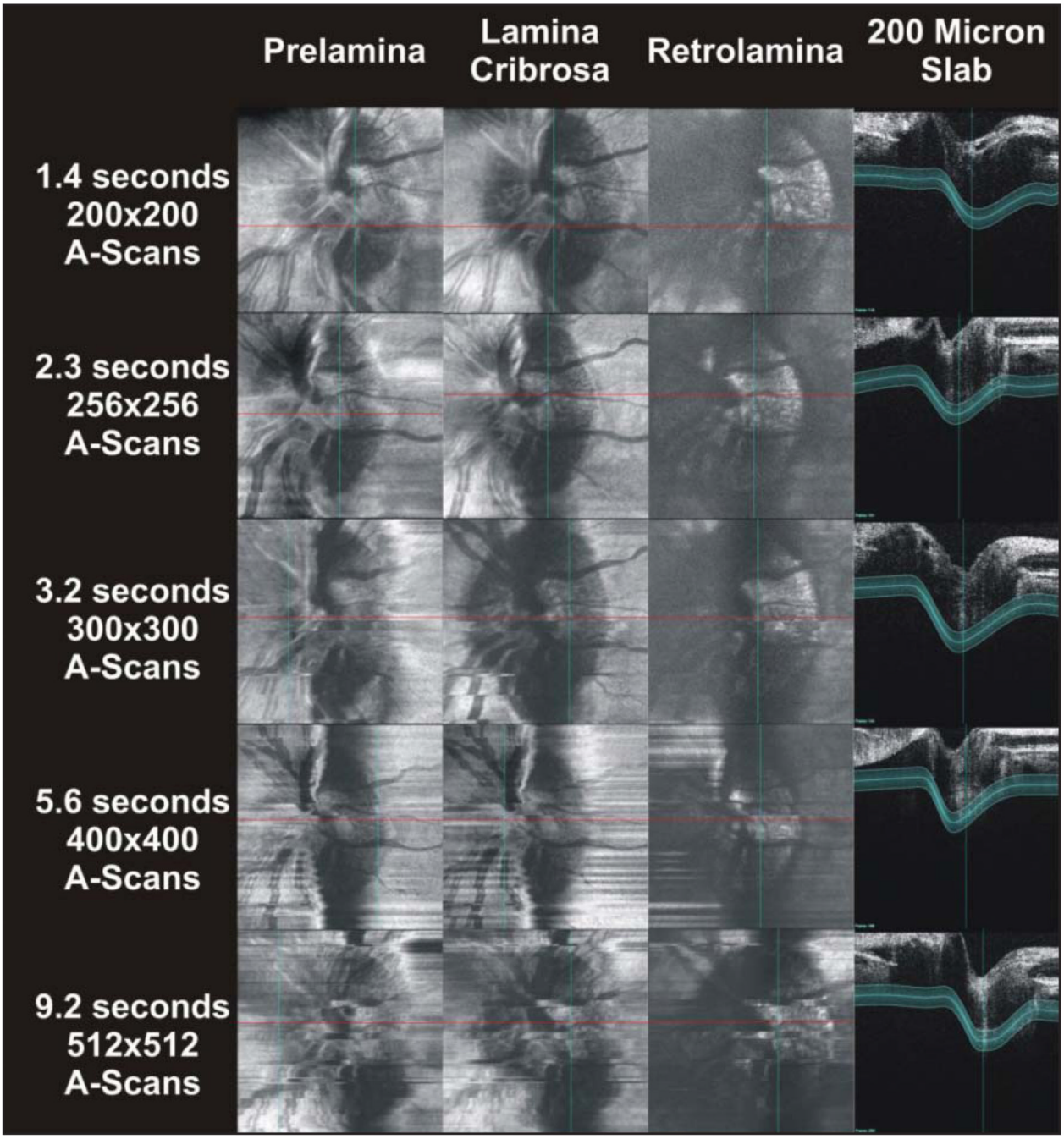

Figure 5.
The effect of increasing A-scan densities, and consequently scan times, on c-mode images and slices. A 200-μm slab was used throughout this image series.

TABLE

Scan Times and Data Sizes for 3D Volumes of Various A-Scan Densities Scanning at 28,000 A-Scans per Second

Scan Density	Scan Time Per Slice (Sec)	Scan Time 3D Volume (Sec)	File Size (MB)	No. of Scans to Fill a 1-TB Drive
200 × 200	0.007	1.4	78	13,422
256 × 256	0.009	2.3	128	8,192
300 × 300	0.011	3.2	176	5,965
400 × 400	0.014	5.6	313	3,355
500 × 500	0.018	8.8	488	2,147
512 × 512	0.018	9.2	512	2,048
750 × 750	0.026	19.7	1,099	954
1,024 × 1,024	0.036	36.7	2,048	512